

Design of an Optimal Preamplifier of Photoplethysmogram for Age-Related Vascular Stiffening Evaluation

Jeom Keun Kim¹, Jae Mok Ahn^{2,*}

^{1,2} Professor, College of Software, Hallym University, 1 Hallymdaehak-gil, Chuncheon-si, Gangwon-do, 24252 South Korea.

*Corresponding author

OCRID: 0000-0002-1061-217X (Jae Mok Ahn)

Abstract

Vascular stiffening is determined with age by evaluating peripheral vascular disease from photoplethysmograms (PPGs). PPG technology has been applied in measurements of oxygen saturation and blood pressure and assessments of various atherosclerotic pathologies and cardiovascular diseases. However, a full understanding of the components of a PPG signal is still lacking because PPGs are very sensitive to motion artifacts, resulting in a poor estimation of the diagnostic value of the different clinical features. Although PPG waveforms are not fully understood, recent studies have focused on investigating the potential information provided by a PPG waveform signal beyond pulse oximetry and heart rate calculations. Therefore, in this study, an optimal transfer function for minimizing artifacts in the preamplifier at the initial state of optical detection was proposed to improve the estimation of the characteristic features of the PPG waveform. Optimal filtering by a simple analog electronic circuit with a fourth-order bandpass filter between the characteristic frequencies, 0.5 Hz-7.5 Hz, and automatic control was implemented. To evaluate the filter performance, three derivatives derived from PPGs were measured. The simulated results were very close to the measured responses. Therefore, the proposed filter enhanced the performance of the motion artifact algorithm for feature extraction and provided a better vascular-related feature estimate.

Keywords: photoplethysmogram, vascular, impulse response, bandpass filter, preamplifier

1. INTRODUCTION

Photoplethysmography (PPG) is a simple optical technique for detecting blood volume changes in the microvascular bed of tissue [1-3]. PPG is being used increasingly more frequently not only in many medical devices but also in smartphones and wearable devices for the assessment of oxygen saturation, cardiovascular disease symptoms, and heart rate variability (HRV). PPG sensors are based on the emission of infrared, green, or red light by an LED that penetrates the skin and blood vessels and measures changes in light absorption [4-5]. The waveform from the PPG sensor is based on changes in transmitted light due to changes in arterial volume and dimension. Thus, PPG technology reflecting a measure of

changes in blood volume in the underlying vascular bed of tissue has been used in various health monitoring systems [6-9]. However, one of the major shortcomings of PPG-based monitoring techniques in healthcare systems is their difficulties in obtaining a stable PPG signal. This limitation is attributable to the fact that the PPG signals are very susceptible to motion artifacts caused by body movements. Motion artifacts have been shown to be a limiting factor attracting many studies related to health monitoring systems using PPG signals, as PPG signals have many potential clinical applications. In HRV estimation technology, the accurate detection of the heartbeat interval used in autonomic nervous system (ANS) evaluation is crucial for successful and precise HRV analysis. HRV indices are traditionally obtained by calculating the R wave peaks of the QRS complexes in ECGs. ECGs measure the electrical activity of the heart by using electrodes placed on the skin. When the heart contracts and pumps blood, a series of coordinated electrical signals are sent to the heart by the ANS. ECG-based measurements are generally accurate within a couple of milliseconds, making it a highly reliable measure of heart rate. The heartbeat interval of two successive R waves (RRI) in an ECG is believed to provide more accurate RRI than estimations based on a finger-type PPG [10]. However, the conventional ECG measurement is uncomfortable and inconvenient. The measurement requires the attachment of at least two cutaneous electrodes on the body surface, with metal components causing skin irritation in some subjects. For this reason, many studies have attempted to develop heart rate monitoring techniques based on PPG measurements, which are simple, low-cost, and easy-to-use alternatives to ECGs [8,11-13]. As a PPG is an indirect optical technique that does not reflect the heart's true activity occurring at its source, it is not always accurate at the millisecond level, but there is an increasing demand for methods of measuring changes in blood volume in the underlying vascular bed of tissue and for a portable system that derives beat-by-beat cardiac rhythm by placing a single sensor on the finger. A fingertip PPG signal is obtained by irradiating the skin surface at a specific wavelength using a light emitting diode (LED) source and detecting the intensity of the transmitted light using a photodiode opposite to the LED. The wavelength and distance between the light source and the photodiode determine the penetration depth of the light. Light with a wavelength from 500 to 1100 nm (from green to infrared) can be used in PPG measurements. Green LEDs have the advantage of demonstrating large variations in intensity by

pulsatile absorption of the blood; however, green LEDs have the disadvantage of having high sensitivity to body movement [14-15]. In contrast, infrared LEDs detect deep-tissue blood flow but are susceptible to changes in the volumes of blood in the peripheral vessels. Red LED light has moderate absorptivity for oxyhemoglobin and deoxyhemoglobin compared with green and infrared LEDs [16-17]. Red LEDs penetrate deeply into the body, delivering a rich source of physiological signals. In this study, red LEDs as a light source were used to develop an optimal filter for preamplification. To use PPG technology for more medical applications, motion artifacts must be reduced to enhance the signal-to-noise ratio through various filtering methodologies [18-19]. While some analysis procedures are common, such as using filters to extract components in a specific frequency range, the different properties of PPG-based biological signals always require the application of vastly different analysis procedures. Hence, it is very useful to investigate the fundamental details of how optimal analog filter for preamplification is carried out before extracting the required information in a microcontroller. We have developed an optimal transfer function as a key method of filtering characteristics, which includes a digital infinite impulse response bandpass filter (IIR BPF), to accurately detect changes in blood volume and heart rate.

2. PPG WAVEFORM

Figure 1 shows a typical PPG waveform and various features when noises have been removed and amplified through both analog and digital signal procedures. The PPG waveform consists of a pulsatile (AC) physiological waveform, which is superimposed on a slowly varying (DC) waveform related to respiration [20]. The maximum point (p1) of the systolic amplitude represents cardiac changes in the blood volume caused by arterial blood flow with each heartbeat. The DC components vary at a slow pace due to respiration, vasoconstrictor fluctuations, and thermoregulation [21-22]. The pulse period of the PPG waveform is divided into two phases. The first rising phase represents stroke volume, which could indicate vasoconstriction or vasodilation. The second falling phase from the p1 point to the next foot point is characterized by diastolic and wave reflections from the periphery. The dicotic notch observed in the diastolic phase stems from the sudden closing of the aortic valve, resulting in retrograde flow and an increase in blood volume in the large artery for a very short time. A dicotic notch is usually observed in the catacrotic phase (second phase) of subjects with healthy compliant arteries. Hence, waveform features such as rise time, amplitude, duration, and various shapes can predict clinically relevant vascular changes in the blood vessels. More detailed

indices of a PPG waveform include the elasticity index, cardiac ejection elasticity index, dicotic index, inflection index, pulse height, time duration (crest time) from the foot of the PPG waveform to its peak, time delay (delta time) between the early systolic peak (p1) and late systolic peak (p2), and pulse period. Crest time provides an important index in the diagnosis of cardiovascular diseases. Crest time is prolonged in patients with vascular disease or hypertension. The vascular stiffness index depends on the height and age of the individual and is associated with delta time (Delta_T), as shown in Figure 1. To extract all information from the PPG waveform, the pulse contour obtained from a noiseless signal must be explained after normalization to the heart rate and height of subjects [23]. To facilitate its interpretation of this contour, many studies have extracted derivatives of the PPG waveform. Figure 2 shows the wave contour of an original PPG signal (left top) and the first (right top), the second (left bottom), and the third (right bottom) derivatives of the PPG signal. The signal's third derivative plays a crucial role in extracting features of the PPG signal's second derivatives because the third derivative identifies whether the second derivative is increasing or decreasing. The third derivative is determined directly from the second derivative. The second derivative of the PPG waveform is called the acceleration plethysmogram (APG) rather than PPG. The peaks in the APG signals are more clearly defined than the peaks in the PPG signals. The APG signal consists of four systolic waves and one diastolic wave: a-peak (early systolic positive peak), b-peak (early systolic negative peak), c-peak (late systolic reincreasing peak), d-peak (late systolic redecaying peak), and e-peak (early diastolic positive peak). The aTime, bTime, cTime, dTime, and eTime are calculated and included in the analysis of age-related vascular status, as shown in Figure 2.

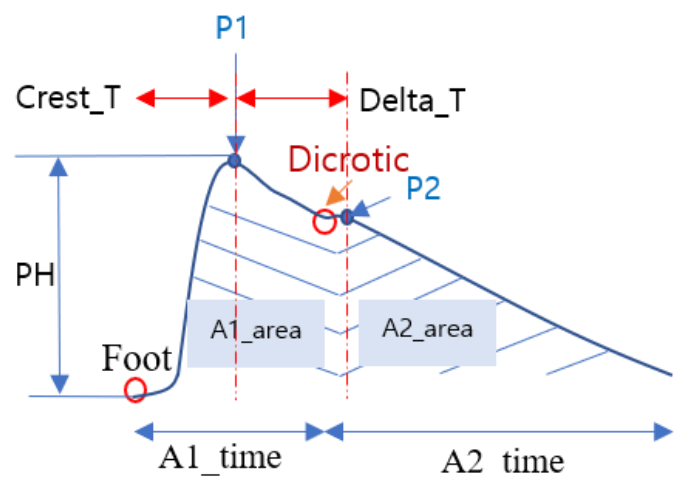


Figure 1. Features of PPG waveform

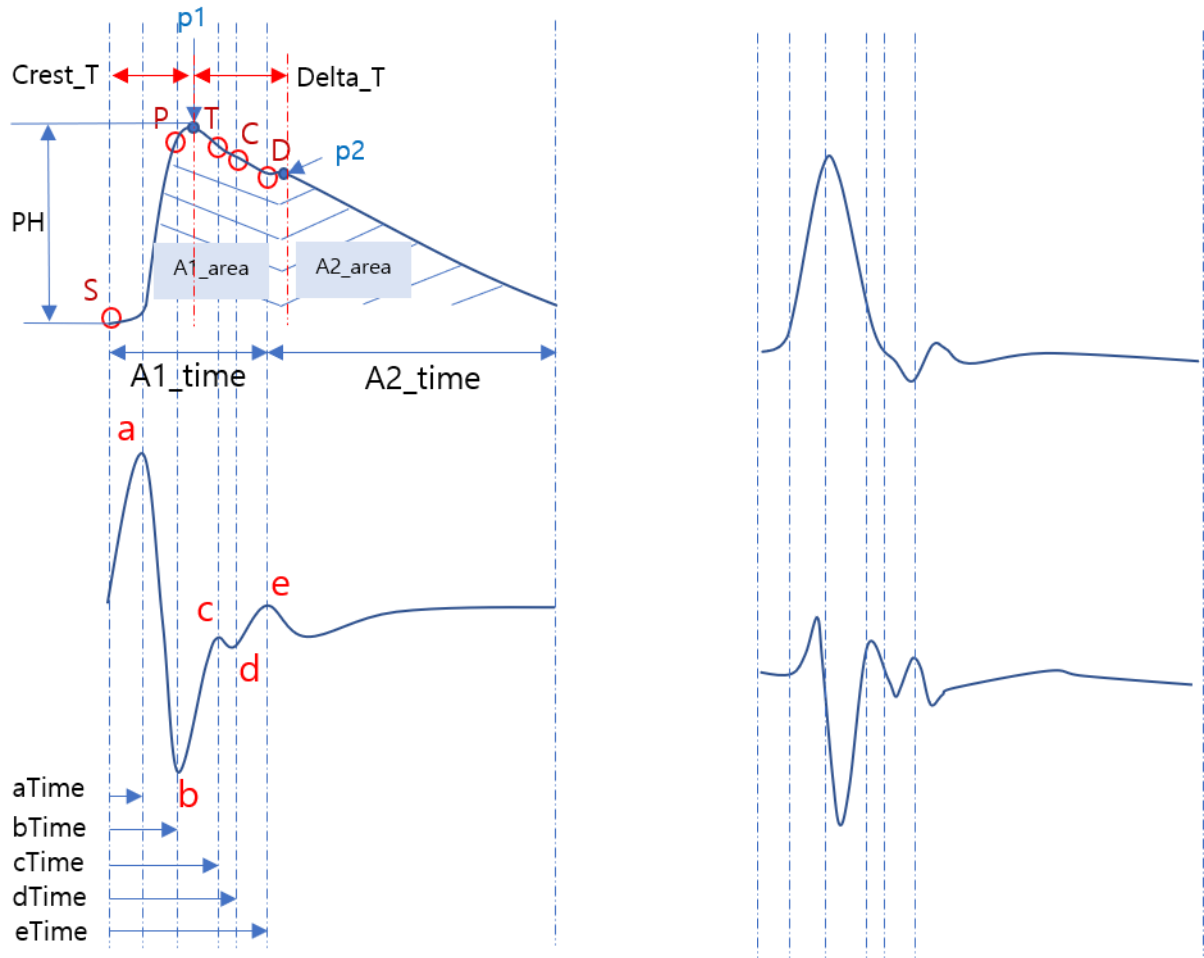


Figure 2. Derivatives of a PPG waveform for the extraction of all features of a PPG waveform: (left top) origin of the PPG, (right top) the first derivative, (left bottom) the second derivative, and (right bottom) the third derivative.

3. MEASUREMENT SYSTEM

The system configuration consists of three components: an analog bandpass filter in the preamplifier that includes a microcontrolled IIR bandpass filter, all derivatives of the signal, and all features of the PPG waveform as shown in Figure 3. In general, the PPG waveform exhibits sudden amplitude changes due to a loss of central blood pressure, constriction of the arterioles, or body movement. Detection of the heart rate and features in very low amplitude PPGs is considered very difficult because low amplitudes affect the quality of the waveform. This study applied a digitally automatic gain controller based on a microcontroller (MSP430F6638, Texas Instruments Company, USA) to respond to such an abrupt change, preventing the amplitude of the PPG from saturating at a maximum or minimum value. As low amplitudes are caused by the breathing process, the range of the respiratory frequencies is from 0.04 to 1.6 Hz, and the frequency of the common motion artifacts is approximately 0.1 Hz. Meanwhile, the waveform frequency of the PPG signal ranges from 0.5 to 4.0 Hz [24-25]. Most motion artifact frequencies, including that of a breathing cycle, are within the frequency range of a PPG signal, which makes it difficult to completely remove noise

from the PPG waveform. Therefore, a schematic diagram consisting of the optimal filtering method and preamplifier with an amplification circuit for medical applications using PPG-based measurements was proposed to obtain high signal quality without signal distortion, as shown in Figure 3. The electric signal captured in the photodiode of the receiver in the fingertip PPG sensor is filtered with a low-pass filter with a cutoff frequency of 100 Hz to remove high frequency noise. A high-pass filter with a cutoff frequency of 0.3 Hz was applied to eliminate the DC components of the signal. Pulse filtering was performed by means of a simple analog electronic circuit with a Sallen-Key low-pass filter with a cutoff frequency, of 7.5 Hz (-3 dB points). The filtered signal is amplified in an operational amplifier with a signal gain of 100. After this analog preprocessing step, the filtered PPG waveform is inputted to a microcontroller to digitally calculate derivatives and extract the features.

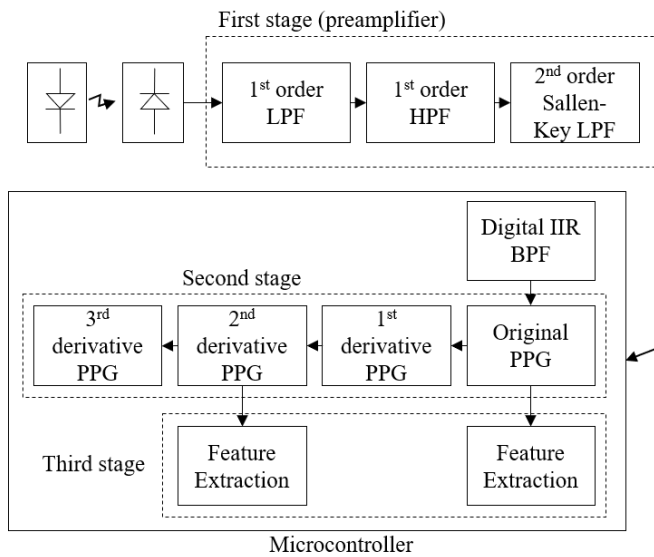


Figure 3. Schematic diagram of the measurement system.

4. DIGITAL IIR BANDPASS FILTER

A recursive IIR digital filter approximates a prototype analog filter defined by the continuous Laplace transfer function $H(s)$ with a discrete filter whose transfer function is $H(z)$. Here, bilinear transformation is used to substitute a function of z for s in $H(s)$ to obtain $H(z)$. The transfer function maps the entire s -plane to the z -plane, enabling us to completely avoid frequency-domain aliasing problems. When the transfer function of a prototype analog filter is $H(s)$, we can obtain the discrete IIR filter z -domain transfer function $H(z)$ by substituting the following for s in $H(s)$,

$$s = \frac{2}{T} \left(\frac{1-z^{-1}}{1+z^{-1}} \right) \quad (1)$$

where, T is the discrete filter's sampling period ($1/f_s$).

To avoid filter instability in the IIR filter design, the z -plane poles should not lie outside the unit circle, which can be prevented by setting the real part to zero ($\sigma=0$) at $s=\sigma+j\omega_a$. Bilinear transformation yields a nonlinear relationship between the analog frequency ω_a and digital frequency ω_d . The frequency response of a digital filter is defined by setting $z = e^{j\omega_d T}$.

$$s = j\omega_a = \frac{2}{T} \frac{1-e^{-j\omega_d T}}{1+e^{-j\omega_d T}} = \frac{2}{T} \frac{e^{j\omega_d T/2} - e^{-j\omega_d T/2}}{e^{j\omega_d T/2} + e^{-j\omega_d T/2}} \quad (2)$$

$$\omega_a = \frac{2}{T} \tan \frac{\omega_d T}{2} \quad (3)$$

Equation 3 shows a nonlinear relationship between the z -domain (digital) frequency and s -domain (analog) frequency. The cutoff frequencies of a digital filter are tangentially warped compared with the cutoff frequencies of an analog filter. To make the practical use of this frequency warping phenomenon,

the s -plane and z -plane frequencies must be related to a more practical f_s (sampling frequency).

$$2\pi f_d = 2 \tan^{-1} \left(\frac{2\pi f_a T}{2} \right) \quad (4)$$

Substituting $1/f_s$ for T , the following equation (5) can be obtained.

$$f_d = \left(\frac{2}{2\pi} \right) \tan^{-1} \left(\frac{2\pi f_a / f_s}{2} \right) = \frac{\tan^{-1} \left(\frac{\pi f_a}{f_s} \right)}{\pi} \quad (5)$$

The expression of a digital filter is an LTI (linear time invariant) system based on the differential equation (6), which is called an IIR filter.

$$y[n] = -\sum_{k=1}^N a[k]y[n-k] + \sum_{k=0}^M b[k]x[n-k] \quad (6)$$

The transfer function for $H(z)$ as shown in equation (7-10) is defined by the differential equation (6).

$$H(z) = \frac{b_0 + b_1 z^{-1} + b_2 z^{-2} + \dots + b_M z^{-M}}{1 + a_1 z^{-1} + a_2 z^{-2} + \dots + a_N z^{-N}} \quad (7)$$

$$H(z) = \frac{B(z)}{A(z)} \quad (8)$$

where

$$B(z) = \sum_{n=0}^M b[n]z^{-n} \quad (9)$$

$$A(z) = 1 + \sum_{n=0}^N a[n]z^{-n} \quad (10)$$

$H(z)$ can be written as

$$H(z) = \frac{z^{-M}}{z^{-N}} \cdot \frac{b_0 z^M + b_1 z^{M-1} + b_2 z^{M-2} + \dots + b_M}{z^N + a_1 z^{N-1} + a_2 z^{N-2} + \dots + a_N} \quad (11)$$

The zeroes of $H(z)$ are the roots of the polynomial in equation (12).

$$b_0 z^M + b_1 z^{M-1} + b_2 z^{M-2} + \dots + b_M \quad (12)$$

The poles of $H(z)$ are the roots of the polynomial in equation (13).

$$z^N + a_1 z^{N-1} + a_2 z^{N-2} + \dots + a_N \quad (13)$$

The details of the implementation of a digital IIR BPF were investigated in our previous paper [26].

5. TRANSFER FUNCTION

The circuit topology is shown in Figure 4. In the first stage except for an optical sensor element, a first order low-pass filter is applied, and a first order high-pass filter used in the next stage in the following equations.

$$|H_o(j\omega)| = \frac{1}{\sqrt{1+(\omega R_1 C_1)^2}}, H_o(s) = \frac{1}{1+sR_1 C_1} \quad (14)$$

$$|H_1(j\omega)| = \frac{\omega R_2 C_2}{\sqrt{1+(\omega R_2 C_2)^2}}, H_1(s) = \frac{sR_2 C_2}{1+sR_2 C_2} \quad (15)$$

The stages compose a simple first-order RC circuit. In the last stage, the low-pass filter in the Sallen-Key architecture is designed as an active filter as well to provide a unit gain. The Sallen-Key configuration shows the least amount of dependence of filter performance on the performance of the operational amplifier. Since the configuration has two sets of RC networks, cutoff frequency for a Sallen-Key is calculated following equation (16).

$$f_c = \frac{1}{2\pi\sqrt{R_3R_4C_3C_4}} \quad (16)$$

As the operational amplifier is configured as a unity gain buffer (A=1), the f_c and output signal magnification Q-factor are completely independent of each other making for a simpler filter design. Then the magnification factor, Q is calculated as:

$$Q = \frac{1}{3-A} = 0.5 \quad (17)$$

The transfer function of a Sallen-Key low-pass filter for the estimation of all R and C values is given as:

$$H_{rc}(s) = \frac{1}{1 + \omega_c C_3(R_3 + R_4)s + \omega_c^2 R_3 R_4 C_3 C_4 s^2} \quad (18)$$

This transfer function makes it much easier to analyze the circuit. From equation (18), given C3 and C4, the resistor values for R3 and R4 are calculated as follows:

$$R_{3,4} = \frac{k_1 C_4 \mp \sqrt{k_1^2 C_4^2 - 4k_2 C_3 C_4}}{4\pi f_c C_3 C_4} \quad (19)$$

To calculate the real values under the square root, C4 must

satisfy the following condition:

$$C_4 \geq C_3 \frac{4k_2}{k_1^2} \quad (20)$$

where the coefficient comparison between the transfer function, $H_{rc}(s)$ in equation (18) and equations (19-20) yields

$$k_1 = \omega_c C_3 (R_3 + R_4) \quad (21)$$

$$k_2 = \omega_c^2 R_3 R_4 C_3 C_4 \quad (22)$$

From the established coefficients of a second-order Butterworth filter, k_1 and k_2 are selected as $k_1=1.4142$ and $k_2=1$. A second-order unity gain Butterworth low-pass filter with a cutoff frequency of $f_c = 7.5$ Hz is designed. $R_3 = R_4 = 15k$ and $C_3 = 1\mu F$ and $C_4 = 2\mu F$ were determined through equations (19-22). Then, the transfer function for the frequency response of the filter is obtained:

$$H_2(s) = \frac{1}{1 + C_3(R_3 + R_4)s + R_3 R_4 C_3 C_4 s^2} \quad (23)$$

The transfer function for the entire circuit in the preamplifier is approximately the product of three separate transfer functions,

$$H_{total}(s) \triangleq H_o(s) \times H_1(s) \times H_2(s) \quad (24)$$

$$H_{total}(s) \triangleq \frac{1}{1 + sR_1C_1} \times \frac{sR_2C_2}{1 + sR_2C_2} \times \frac{1}{1 + C_3(R_3 + R_4)s + R_3 R_4 C_3 C_4 s^2} \quad (25)$$

Figures 5 and 6 show the frequency response of the total transfer function used in the preamplifier and a pole-zero representation of the left side of the s-plane used to ensure filter stability, respectively.

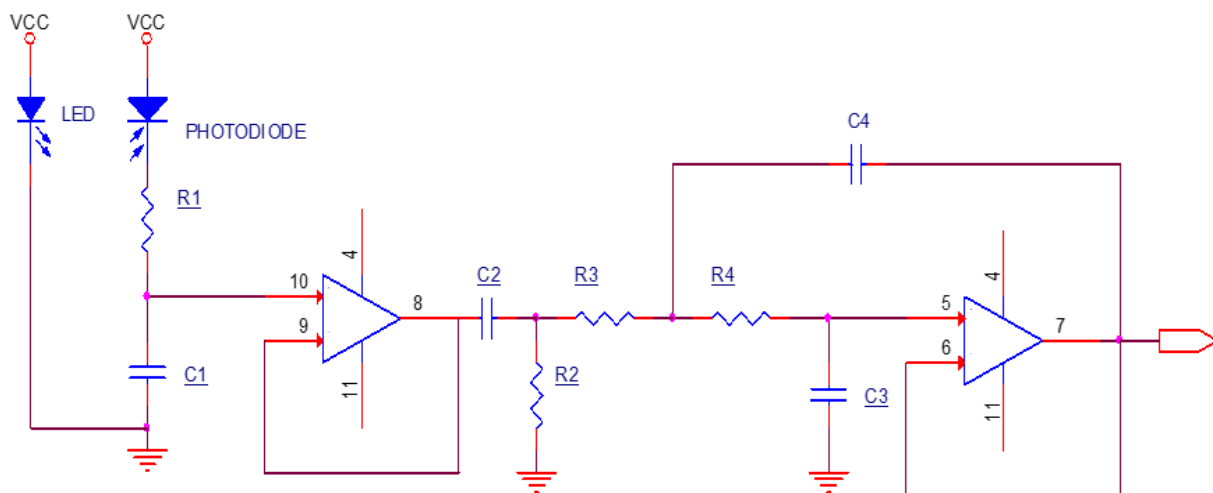


Figure 4. Basic circuit topology

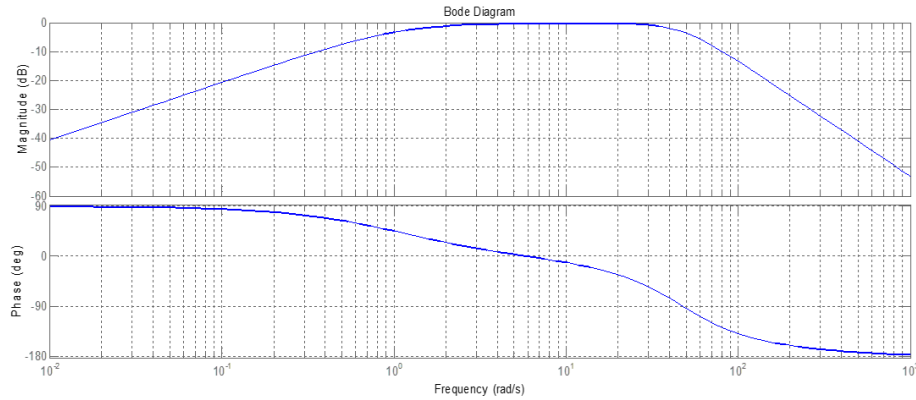


Figure 5. A Bode plot of the frequency response of $H_2(s)$ used to achieve a bandpass filter in the preamplifier: (top) magnitude and (bottom) phase vs. frequency in a log scale.

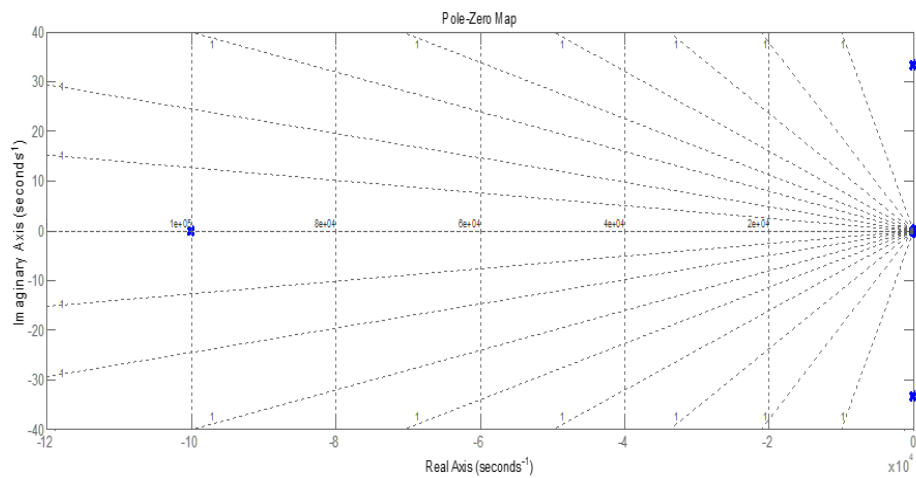


Figure 6. A pole-zero representation of the s-plane of the continuous model, $H_{total}(s)$.

6. RESULTS

The results of the filtered PPG timeseries obtained by implementing the signal conditioning stages, including a low-pass filter, a high-pass filter, a Sallen-Key low-pass filter, a digital IIR BPF, and additional amplification are presented in Figure 7. The recording is from the index finger site over a period of 10 seconds using HRV analyzer (TAS9VIEW, IEMBIO. Ltd., Chuncheon-si, South Korea). A careful analysis of the third derivative of the PPG signal allowed the detection of the maximum and minimum points of the PPG waveform. In Figure 7, the top wave represents the original PPG, the second wave represents the first derivative, the third wave represents the second derivative, and the fourth wave represents the third derivative. Figure 7(c) shows the functional index based on vascular distensibility and the degree of vascular stiffening from the second derivative of the PPG signal. The acceleration photoplethysmogram (APG) reflecting the PPG's second derivative was used as an aging index that reflects vascular morphology. The 3rd derivative as shown in Figure 7(d) was utilized for the detection of the maximum and minimum points

of the APG waveform. All derivatives except for the source PPG signal were generated by a digital signal processing algorithm that included a digital IIR BPF based on a microcontroller. A photodetector directly passed the signals to an electronic circuit with an operational amplifier that includes a transimpedance amplifier before inputting them to a low-pass filter circuit. Next, a high-pass filter reduced the magnitude of the DC component and finally, the Sallen-Key low-pass filter enabled the pulsatile AC component to be increased to 1.2 V at the peak-to-peak level on average, spontaneously changing within the range of 50 mV to 2.5 V. The PPG signal with a stable amplitude was quickly maintained by a smart autogain controller inside the microcontroller. The high-pass filter cutoff frequency was carefully selected: excessive filtering can distort the pulse waveform, but insufficient filtering can result in the DC component dominating the pulsatile wave. Consequently, relevant physiological features were defined by detecting the characteristic points on the PPG and APG waveforms for each heartbeat after the developed transfer function and digital IIR BPF removed noise and motion artifacts.

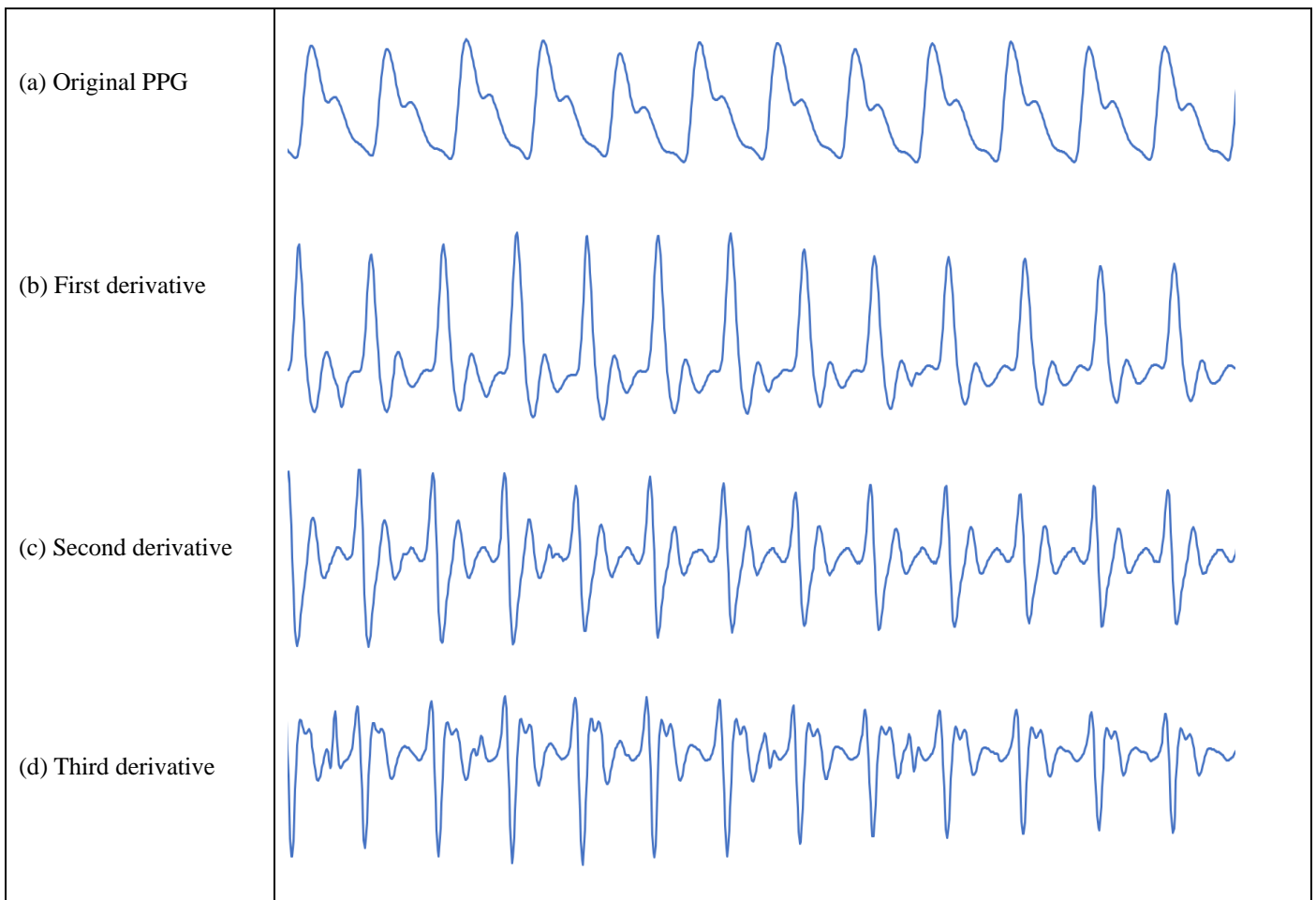


Figure 7. The measured data for (a) an original PPG, (b) the first derivative, (c) the second derivative, and (d) the third derivative after filtering with the proposed transfer function and the digital IIR BPF based on a microcontroller was completed.

7. CONCLUSIONS

In this work we presented an optimal transfer function for the preamplification of PPG-based measurements for the assessment of age-related vascular health. The signal artifacts of the PPG waveform related to electronic noises, signal distortion, random noise, and sensor issues have been improved following the implementation of the proposed optimal transfer function in the preamplifier. Therefore, we can obtain robust medical indicators calculated inside a microcontroller from a source PPG waveform. The extraction of all PPG features related to the cardiovascular system and atherosclerosis in the artery was carried out and verified. In general, when the PPG signal is differentiated, a noiseless smooth curve cannot be obtained without a clear source signal. However, in this study an acceptable PPG signal could be achieved even though the third derivative was used. The main design of the transfer function was based on robust signal processing and a microcontroller to easily recognize specific features of the PPG waveform. The combination of the proposed transfer function and a digital IIR BPF can effectively enhance the quality of the signal; it can yield a signal with a stable amplitude and remove the DC components imposed on the PPG signal. Even a small change in volume caused by a pulse with low blood pressure

can be easily detected in the optical amplifier by penetrating the body deeply with red light from a light-emitting diode (LED) and then measuring the amount of light transmitted to the photodiode. Recently, PPG-based measurements have been applied in a wide range of commercially available medical devices for detecting peripheral vascular disease and evaluating autonomic function based on heart rate variability technology. Nevertheless, challenges remain with PPG-based technology, including the removal of motion artifacts in various surrounding environments, the use of a fast automatic gain controller in response to an abrupt change in the amplitude, or synchronous movements related to breathing, and the standardization of measurements. Future studies should develop transfer functions for specific motion artifacts by analyzing the correlation between the PPG signal, the motion artifact patterns, and the ambient environment.

ACKNOWLEDGEMENTS

This work was supported by the Hallym University Research Fund (HRF-201901-012).

REFERENCES

- [1] Allen, J. Photoplethysmography and its application in clinical physiological measurement. *Physiological measurement*, 28(3), R1-R39 (2007).
- [2] Elgendi, M. On the analysis of fingertip photoplethysmogram signals. *Current Cardiology Reviews*, 8, 14-25 (2012).
- [3] Takazawa, K., Tanaka, N., Fujita, M., Matsuoka, O., Saiki, T., Aikawa, M., Tamura, S., Ibukiyama, C. Assessment of vasoactive agents and vascular aging by the second derivative of photoplethysmogram waveform. *Hypertension*, 32(2), 365-370 (1998).
- [4] Giardino, N.D., Lehrer, P.M., Edelberg, R. Comparison of finger plethysmograph to ECG in the measurement of heart rate variability. *Psychophysiology*, 39(2), 246-253 (2002).
- [5] Anderson, R.R., Parrish, J.A. The optics of human skin. *Journal of Investigative Dermatology*, 77(1), 13-19 (1981).
- [6] Peng, R.C., Zhou, X.L., Lin, W.H., Zhang, Y.T. Extraction of heart rate variability from smartphone photoplethysmograms. *Computational and Mathematical Methods in Medicine*, 2015(1), 1-11 (2015).
- [7] Tamura, T., Maeda, Y., Sekine, M., Yoshida, M. Wearable photoplethysmographic sensors-past and present. *Electronics*, 3, 282-302 (2014).
- [8] Gil, E., Orini, M., Bailon, R., Vergara, J.M., Mainardi, L., Laguna, P. Photoplethysmography pulse rate variability as a surrogate measurement of heart rate variability during non-stationary conditions. *Physiological Measurement*, 31(9), 1271-1290 (2010).
- [9] Charlot, K., Cornolo, J., Brugniaux, J.V., Richalet, J.P., Pichon, A. Interchangeability between heart rate and photoplethysmography variabilities during sympathetic stimulations. *Physiological Measurement*, 30(12), 1357-1369 (2009).
- [10] Ahn, J.M. Heart rate variability (HRV) analysis using simultaneous handgrip electrocardiogram and fingertip photoplethysmogram. *Advances in Information Sciences and Service Sciences (AISS)*, 5(13), 164-170 (2013).
- [11] German-Sallo, Z., German-Sallo, M. Non-linear methods in HRV analysis. *Procedia Technology*, 22, 645-651, (2016).
- [12] Azabji Kenfack, M., Lador, F., Licker, M., Moia, C., Tam, E., Capelli, C., Morel, D., Ferretti, G. Cardiac output by Modflow method from intra-arterial and fingertip pulse pressure profiles. *Clinical Science*, 106(4), 365-369 (2004).
- [13] Mukherjee, R., Ghosh, S., Gupta, B., Chakravarty, T. Reflective PPG-based noninvasive continuous pulse rate measurement and remote monitoring system. *IEEE 2017 Global Wireless Summit (GWS)*, 193-197 (2017).
- [14] Spigulis, J., Gailite, L., Lihachev, A., Erts, R. Simultaneous recording of skin blood pulsations at different vascular depths by multiwavelength photoplethysmography. *Applied Optics*, 46(10), 1754-1759 (2007).
- [15] Meada, Y., Sekine, M., Tamura, T. The advantage of green reflected photoplethysmograph. *Journal of Medical Systems*, 35, 829-834 (2011).
- [16] Nitzan, M., Romem, A., Koppel, R. Pulse oximetry: fundamentals and technology update. *Medical Devices: Evidence and Research*, 7, 231-239 (2014).
- [17] Mannheimer, P.D. The light-tissue interaction of pulse oximetry. *Anesthesia and Analgesia*, 105(6), S10-17 (2007).
- [18] Fischer, C., Domer, B., Wibmer, T., Penzel, T. An algorithm for real-time pulse waveform segmentation and artifact detection in photoplethysmograms. *IEEE Journal of Biomedical Health Informatics*, 21(2), 372-381 (2017).
- [19] Tautan, A.M., Young, A., Wentink, E., Wieringa, F. Characterization and reduction of motion artifacts in photoplethysmographic signals from a wrist-worn device. *37th Annual International Conference of the IEEE Engineering in Medicine and Biology Society*, 6146-6149 (2015).
- [20] Herzman, A.B. Photoelectric plethysmography for the fingers and toes in man. *Experimental Biology and Medicine*, 37, 529-542 (1937).
- [21] Harness, J.B., Marjanovic, D.Z. Low-frequency plethysmograph signals. *Clinical Physics and Physiological Measurement*, 10(4), 365-367 (1989).
- [22] Schultz-Ehrenburg, U., Blazek, V. Value of quantitative photoplethysmography for functional vascular diagnostics. Current status and prospects. *Skin Pharmacology and Applied Physiology*, 14(5), 316-323 (2001).
- [23] Allen, J., Murray, A. Age-related changes in peripheral pulse shape characteristics at various body sites. *Physiological Measurement*, 24, 297-307 (2003).
- [24] Lee, H.W., Lee, J.W., Jung, W.G., Lee, G.K. The periodic moving average filter for removing motion artifacts from PPG signals. *International Journal of Control, Automation, and Systems*, 5(6), 701-706 (2007).
- [25] Lee, J.W., Jung, W.G., Kang, I.T., Kim, Y.I., Lee, G.K. Design of filter to reject motion artifact of pulse oximetry. *Computer Standards & Interfaces*, 26(3), 241-249 (2004).
- [26] Kim, J.K., Ahn, J.M. Design of an optimal digital IIR filter for heart rate variability by photoplethysmogram. *International Journal of Engineering Research and Technology*, 11(12), 2009-2021 (2018).